An X-ray absorption fine structure study of copper(I) chloride coordination structure in water up to 325°C

ARTICLE *in* CHEMICAL PHYSICS LETTERS · NOVEMBER 2000

Impact Factor: 1.9 · DOI: 10.1016/S0009-2614(00)01110-6

3 AUTHORS, INCLUDING:

John G. Darab
MEL Chemicals
83 PUBLICATIONS **1,575** CITATIONS

10 November 2000

ELSEVIER

Chemical Physics Letters 330 (2000) 300–308

CHEMICAL PHYSICS LETTERS

www.elsevier.nl/locate/cplett

An X-ray absorption fine structure study of copper(I) chloride coordination structure in water up to 325°C

John L. Fulton *, Markus M. Hoffmann, John G. Darab

Environmental and Health Sciences Division, Pacific Northwest National Laboratory [1], Battelle Boulevard, P.O. Box 999, Richland, WA 99352, USA

Received 21 July 2000; in final form 18 September 2000

Abstract

X-ray absorption fine structure (XAFS) spectroscopy was used to measure the Cl^- and H_2O coordination structure about Cu^{1+} in water at temperatures up to 325°C including the coordination numbers, symmetry, distances and the amount of bond disorder. The linear dichloro Cu^{1+} species, $[CuCl_2]^-$, is especially stable and it is predominant from 100°C to 325°C in the presence of excess Cl^-. Even for solutions with 2.0 m NaCl, only the dichloro Cu^{1+} species is observed with no evidence of higher Cl^- coordination. There is no evidence of hydration waters in the first-solvation shell of this dichloro-species.

1. Introduction

The oxidation/reduction and coordination chemistry of Cu^{1+}/Cu^{2+} underlies many important biological, geochemical and industrial processes. Specific oxidation states can be stabilized by the types of the coordination chemistry about the cation. In water at elevated temperatures, Cu(I) is often thermodynamically more stable than Cu(II). In this communication, we report the unusual structure of a $CuCl_2^-$ species in water at temperatures from 100°C to 325°C. The method used in this characterization is X-ray absorption fine structure spectroscopy (XAFS) which accurately measures the first-shell structure about ions. For aqueous systems, an understanding of this first-shell structure is paramount to defining the controlling thermodynamics of the system. Only recently has the utility of this technique been realized for probing aqueous systems well above 200°C [1–9].

At elevated temperatures, it is possible to increase the cation-to-anion coordination without changing the chemical composition of the systems [7]. At moderate-to-low concentrations and under ambient conditions, most cations and anions would normally be fully dissociated. However, at high temperatures the contact-ion pairs form. Thus, for aqueous systems containing simple salts, one can explore both the hydration and the contact-ion-pair chemistry. In contrast, the chemistry of organic ligands is a great deal more complex because the symmetry and binding are strongly influenced by the structure of the ligand. Hence, the coordination structure derived from these simple aqueous solutions is relevant to building a better understanding of the coordination chemistry

* Corresponding author. Fax: +1-509-376-0418.
E-mail address: john.fulton@pnl.gov (J.L. Fulton).

[1] Operated by Battelle Memorial Institute.

0009-2614/00/$ - see front matter
PII: S0009-2614(00)01110-6

of Cu^{1+} to large organic ligands or to biomolecules. Furthermore, these results are also of interest for comparison to ab initio and density functional methods because of the simple nature of the ligand structure.

Aqueous Cu^{1+} species have low solubility in water under ambient conditions making their study difficult. However, the $[CuCl_2]^-$ species is soluble in polar organic liquids such as acetonitrile and dimethyl sulfoxide under ambient conditions where it is reported to have a Cu–Cl bond distance of 2.10 Å [10]. An interesting and surprising finding from the same studies is that the $[CuCl_2]^-$ species has no coordination with the polar solvent in the first shell. Under hydrothermal conditions Cu^{1+} species are often thermodynamically favored and it is known that $[CuCl_2]^-$ is an important species for transport of copper in geochemical systems [11,12]. In this Letter, we show that the linear $[CuCl_2]^-$ species is thermodynamically favored under hydrothermal conditions.

2. Experimental details

The Cu XAFS spectra were acquired in a high-pressure cell constructed from a 2 mm long tube of copper metal and two diamond windows that allowed for the transmission of the X-ray beam. Details of the design have been provided elsewhere [13–15]. The only cell surfaces in contact with the high-temperature copper solution were high purity copper metal (the reductant in the reaction with Cu^{2+}) and diamond. This design circumvents difficulties of reactions of Cu^{2+} with other cell or seal materials since the highly reactive Cu^{2+} has been shown to readily oxidize Pt metal [13]. All solutions were deoxygenated by purging with N_2 prior to use. The aqueous solutions containing $CuCl_2$, NaCl and HCl, were loaded into the cell under ambient conditions. In order to reduce the likelihood of copper hydrolysis reactions at 325°C the starting solutions were acidified with HCl to a starting pH of at least 1.5 prior to heating. After introducing the solution into the cell with a micropipet, the top single-crystal diamond window was installed and pre-loaded with a force against the copper ring. This pre-load force was sufficient to seal the internal liquid phase at the vapor pressure up to 325°C.

As our study finds, the reduction of Cu(II) to Cu(I) occurs immediately at temperatures near and above 100°C according to one of the two following chemical reactions that depend upon the initial total concentration of Cl^-:

$$[Cu(H_2O)_6]^{2+} + 4Cl^- + Cu^0 \underset{T \geqslant 100°C}{\rightarrow} 2[CuCl_2]^- + 6H_2O \quad (1)$$

$$[Cu(H_2O)_6]^{2+} + 2Cl^- + Cu^0 \underset{T \geqslant 100°C}{\rightarrow} 2[Cu(H_2O)Cl] + 4H_2O \quad (2)$$

The hexaaqua Cu^{2+} species is very soluble at all temperatures while the dichloro Cu^{1+} species is only soluble at temperatures near or above 100°C. The monochloro monoaqua Cu^{1+} species has relatively low solubility until about 300°C (as determined from the measured Cu edge height at different conditions).

An alternate reaction was also explored for the formation of the $[CuCl_2]^-$ species in which CuO(s) instead of $CuCl_2$ was introduced into the cell

$$CuO + 2H^+ + 4Cl^- + Cu^0 \underset{T \geqslant 100°C}{\rightarrow} 2[CuCl_2]^- + H_2O \quad (3)$$

This reaction was also very rapid at 100°C and analysis of the full XAFS spectra described in the following section indicated that the final Cu oxidation state and coordination was identical to that for the reaction in Eq. (1) under acidic conditions.

Different regions of the XAFS spectra contain different types of chemical and structural information about the aqueous ions. The pre-edge and the X-ray absorption near edge (XANES) regions, from about 20 eV below to about 30 eV above the absorption edge, contain information about the oxidation state and the coordination symmetry. The extended X-ray absorption fine structure (EXAFS) region, from 30 eV to about 1000 eV above the absorption edge, contains the information about the coordination numbers, distances and bond disorder. The copper *K*-edge (8979 eV) XAFS spectra were collected on the insertion device beamline (PNC–CAT) at the Advanced

Photon Source (Argonne National Laboratory). Analysis of the EXAFS data [16–18] were accomplished using well-established methods that are part of the UWXAFS program [19]. The method involves extracting the EXAFS oscillations, $\chi(k)$, from the experimentally measured absorption coefficient where the wavenumber of the ejected photo-electron is given by $k = \sqrt{2m_e(E - E_0)/\hbar^2}$ with E_0 being the absorption edge energy. Details of the procedures for fitting the various structural parameters for copper solutions is identical to that reported previously [13] and is similar to methods also used for nickel solutions [7]. The fitted parameters include, N, the coordination number of the shell, R, the shell distance, σ^2, the Debye–Waller factor, which represents the mean-square variation in R due to both static and thermal disorder, and, finally, C_3, the anharmonicity of the pair-distribution. The fitting of the FEFF theoretical standards [20] to the experimental data was accomplished using an analysis program (FEFFIT) [19,21] that employs a non-linear, least-squares technique.

3. Results and discussion

Fig. 1 illustrates the results for the coordination structure of the Cu^{1+} and Cu^{2+} species derived from this study. The analysis of the XAFS results leading to these structures is discussed here in detail. We start with the analysis of the XANES spectra plotted in Fig. 2. The most prominent feature in these plots is the strong XANES peak at 8984 eV for the three different Cu solutions at temperatures above 100°C as indicated. This peak is absent for the Cu^{2+} solution under ambient conditions. This peak is assigned to the $1s \rightarrow 4p$ transition of the Cu^{1+} species [13] and the relative intensity of the band with respect to known Cu(I) compounds indicates that there is 100% conversion of the Cu(II) to Cu(I) as described by Eqs. (1)–(3). The intensity of this $1s \rightarrow 4p$ transition and its position are also strong indicators of the coordination structure about Cu^{1+} as has been shown in an exhaustive investigation of 19 Cu(I) compounds by Kau et al. [22]. For the solutions shown in Fig. 2, the edge-normalized peak height is between 1.03 to 1.12 for the three high-temperature spectra. The results of Kau et al. [22] report peak heights of 1.08, 0.63 and 0.72 for the 2, 3 and 4 coordinate Cu(I) species, respectively. Thus the results in Fig. 2 strongly indicate that the high-temperature Cu^{1+} species are two-coordinate species. In Fig. 2, for the Cu^{1+} solutions, we also observe the disappearance of the strong XANES peak at 8995 eV for the Cu^{2+} solutions. Since oxygen is a much lower Z atom than chlorine, the Cu–O XAFS amplitude function [7], $F_i(k)$, is larger by about a factor of 5 in this energy region from ~8995–9005 than the Cu–Cl amplitudes. Thus, the disappearance of this intense peak, which is due primarily from Cu–O single scattering and multi-

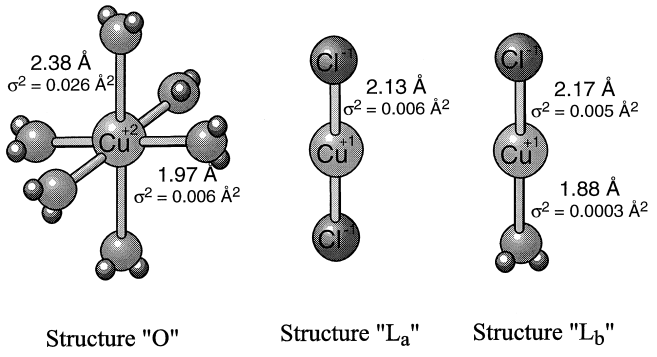

Fig. 1. Schematic structures of the Cu^{2+} and Cu^{1+} hydrothermal species. The waters of hydration about the Cl^- are not shown for clarity. Structure $\mathbf{L}_b$ is shown as a Cu monomer species but, as discussed in the text, a dimer species is also consistent with the XAFS analysis.

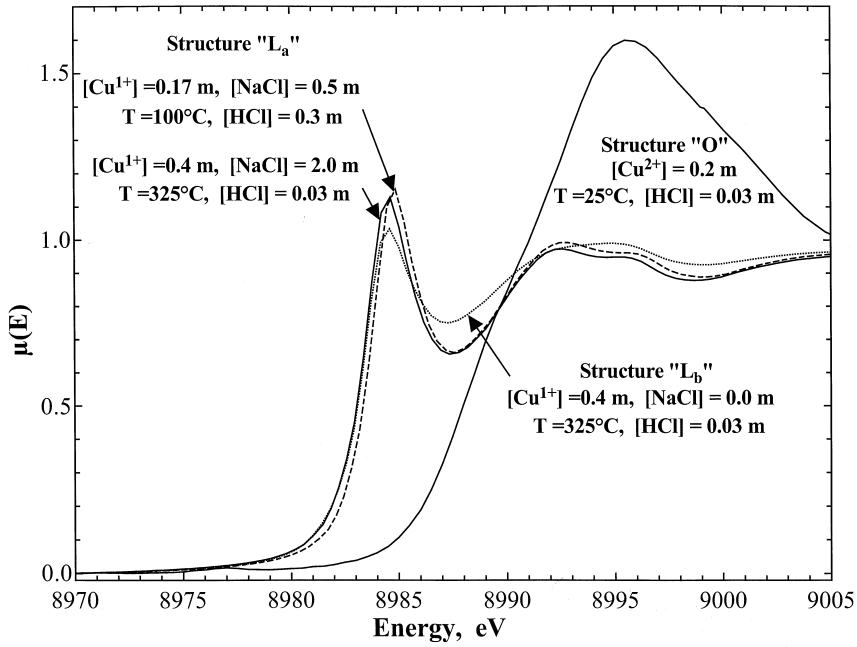

Fig. 2. Pre-edge and XANES spectra at the Cu *K*-edge for the ambient hexaaqua Cu^{2+} species and for three different hydrothermal Cu^{1+} solutions. All spectra have been scaled to a common edge-height.

ple scattering (MS), is consistent with the complete loss of water (O) in the first-coordination shell about Cu^{1+}.

For the hexaaqua Cu^{2+} species, there is a weak transition at 8977 eV that is assigned to the $1s \rightarrow 3d$ transition that is weakly allowed through either quadrapolar [23] coupling or a slight amount of thermal disorder, mixing in *p*-character distortion to destroy the inversion symmetry. The Cu^{1+} state has a closed shell configuration (d^{10}) and thus zero probability of a $1s \rightarrow 3d$ transition. Thus, the three high-temperature spectra in Fig. 2 show no evidence of a peak in this region further confirming that all of the Cu is in the Cu^{1+} state.

We now move on to the analysis of the EXAFS region to extract the coordination number, distances and Debye–Waller factors. Fig. 3 shows the Cu *K*-edge EXAFS spectra (k^2-weighted $\chi(k)$ data) for four different copper solutions from 25°C up to 325°C. The dotted lines shown in Fig. 3 represent the theoretical fits to the experimental data that were used to extract the various structural parameters listed in Table 1. The room temperature spectrum in Fig. 3 corresponds to the well-known structure of the distorted octahedral symmetry with six water ligands illustrated by structure **O** in Fig. 1. There are recent detailed studies of this ambient Cu^{2+} species [24–26] and another study of the Cu^{2+} structure up to 175°C [27].

In Fig. 3, the two middle spectra corresponding to structure $\mathbf{L}_a$ in Fig. 1, are virtually identical even though the conditions are greatly different. The spectra acquired at 100°C has 0.17 m Cu^{1+} and 0.5 m NaCl whereas the spectra acquired at 325°C with 0.4 m Cu^{1+} and 2.0 m NaCl has much higher overall Cu^{1+} and NaCl concentrations. Both higher concentrations and higher temperature should tend to increase the coordination of Cu^{1+} with Cl^-. However, the results show that there is a large area of the phase space, where the stable $\mathbf{L}_a$ structure is present – an equilibrium in agreement with thermodynamic models [11]. The final spectrum in Fig. 3, for the 0.4 m Cu^{1+} solution without added NaCl salt, has slightly different amplitudes and phase shifts than for the other two Cu^{1+} spectra. For this system, the overall ratio of $[Cl^-]/[Cu^{1+}]$ is about 1, whereas for the two preceding solutions $[Cl^-]/[Cu^{1+}]$ is greater than 2.

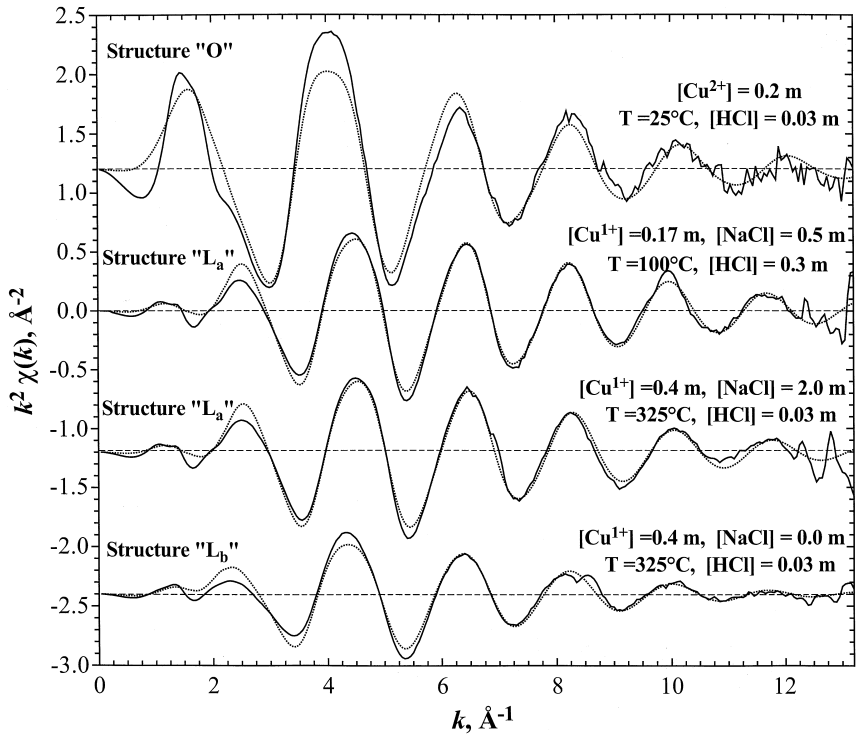

Fig. 3. A Cu EXAFS k^2-weighted $\chi(k)$ plot for the ambient hexaaqua Cu^{2+} species and for three different hydrothermal Cu^{1+} solutions as indicated. The solid line shows the experimental data and the dashed line shows the model fit to the data set using FEFF calculations and the parameters listed in Table 1.

Hence, the species tentatively identified as $\mathbf{L}_b$ (in Fig. 1) is formed under these conditions. Further, for the solution without added NaCl we observed that the concentration of dissolved $\mathbf{L}_b$ Cu^{1+} species was low below about 200°C (e.g., at 200°C only 25% of the available copper dissolved) in contrast to the $\mathbf{L}_a$ species where all available Cu^{1+} dissolved at 100°C. When the temperature of the solution without added NaCl was increased to 325°C all of the available Cu^{1+} dissolved. At each condition the amount of soluble Cu(I) or Cu(II) is determined from the height of the Cu absorption edge.

Fig. 4 gives the $\tilde{\chi}(R)$ results that represent the magnitude of the Fourier transformed $\chi(k)$ data given in Fig. 3. The $\tilde{\chi}(R)$ functions are closely related to the standard radial, partial-pair distribution functions with the caveat that for distances greater than about 4 Å the $\tilde{\chi}(R)$ results are strongly damped by the convolution with the photo-electron scattering functions and by the large disorder for atoms beyond the first shell. Both of these aspects are fully treated by the FEFF code. As in Fig. 3, the dotted lines in Fig. 4 represent the theoretical fits to the experimental data. The primary feature of the $\tilde{\chi}(R)$ plots of Fig. 4 is the large peak near 1.5 Å due to either the oxygen atoms of water ligands or Cl^- ligands bound to the Cu species. The secondary feature is the weak-to-moderate peak between 3 and 4 Å from the collinear MS paths involving the most tightly bound ligands. The MS paths are illustrated in Fig. 4. For the hexaaqua Cu^{2+} species at room temperature, the MS peak at 3.25 Å is due to the collinear MS paths of the equatorial oxygens [24]. For the 100°C Cu^{1+} spectra, the MS peak has moved out to 3.75 Å. In this case, the collinear MS contribution is from the Cl^-–Cu–Cl^- coordination that occurs at a slightly larger distance since the Cl hard-sphere radius is somewhat larger than that of O. In addition, the fitted Debye–Waller factor (Table 1) for

Table 1
Cu(I,II) speciation under hydrothermal conditions[a]

System							Conditions	Structure						$\mathscr{R}$[b]
ID	Species	$[Cu^{2+}]$	$[Cu^{1+}]$	[NaCl]	[HCl]	$[Cl^-]_{total}$	T (°C)	Scatterer	N	R (Å)	$\sigma^2_{SS} \times 10^3$ (Å^2)	$\sigma^2_{MS} \times 10^3$ (Å^2)	$C_3 \times 10^4$	
A	**O**	0.2	0.00	0.00	0.03	0.43	25	Oxygen	4.2(0.3)	1.969(0 0 6)	5.6(0.9)	1.8(3.8)	0.8(1.4)	0.017
								Oxygen	2[c]	2.375(0 3 1)	26.0(9.0)	–	–	–
B	$\mathbf{L}_a$	0.0	0.20	0.50	0.30	0.80	100	Chloride	1.9(0.1)	2.131(0 0 9)	5.3(0.7)	10.9(4.4)	0.0(1.2)	0.022
C	$\mathbf{L}_a$	0.0	0.20	0.50	0.30	0.80	200	Chloride	1.9(0.1)	2.123(0 0 5)	4.9(0.6)	10.2(3.9)	0.1(1.1)	0.019
D	$\mathbf{L}_a$	0.0	0.20	0.50	0.30	0.80	325	Chloride	2.0(0.2)	2.123(0 0 7)	6.0(1.0)	13.7(7.1)	0.0(1.7)	0.038
E	$\mathbf{L}_a$	0.0	0.34	2.0	0.03	2.37	200	Chloride	1.8(0.2)	2.132(0 0 7)	6.0(0.9)	18.8(9.8)	0.1(1.6)	0.032
F	$\mathbf{L}_a$	0.0	0.40	2.0	0.03	2.43	325	Chloride	1.9(0.1)	2.120(0 0 5)	5.9(0.6)	15.7(5.2)	0.0(1.1)	0.015
G	$\mathbf{L}_b$	0.0	0.40	0.00	0.03	0.43	325	Chloride	1.0(0.1)	2.173(0 2 2)	4.8(2.6)	15.7(7.5)	4.3(5.0)	0.015
								Oxygen	0.3(0.2)	1.876(0 5 0)	0.3(5.1)	–	–	–
G	**Dimer**	0.0	0.40	0.00	0.03	0.43	325	Chloride	1.4(0.2)	2.173(0 1 0)	5.5(2.1)	1.8(5.6)[d]	0.2[e]	0.013
								Oxygen	0.5(0.2)	1.966(0 3 1)	3.3(2.5)	–	–	–

[a] Results of Cu XAFS analysis of first-shell Cu(I,II) structures. The predominant species types (**O**, $\mathbf{L}_a$ or $\mathbf{L}_b$) are shown in Fig. 1. The concentrations represent those at the reported conditions and they are expressed in molality. The reported amounts of soluble Cu^{2+} and Cu^{1+} were determined from the edge and pre-edge peak heights at the stated conditions. For experiments 'E', 'F' and 'G' the starting solution contained $CuCl_2$, NaCl and HCl with the formation of the new Cu^{1+} species according to Eqs. (1) and (2). For experiments 'B', 'C' and 'D' the starting solution contained CuO, NaCl and HCl with the formation of the new Cu^{1+} species according to Eq. (3). For experiment 'G' the same experimental data was fit to two different models: a monomer ($\mathbf{L}_b$) and a dimer species as described in the text.
[b] Goodness of fit defined by a scaled sum-of-square as described in the UWXAFS package.
[c] Fixed in the fitting.
[d] For the linear –Cl–Cu–H_2O portion of the dimer.
[e] Fixed in the fitting.

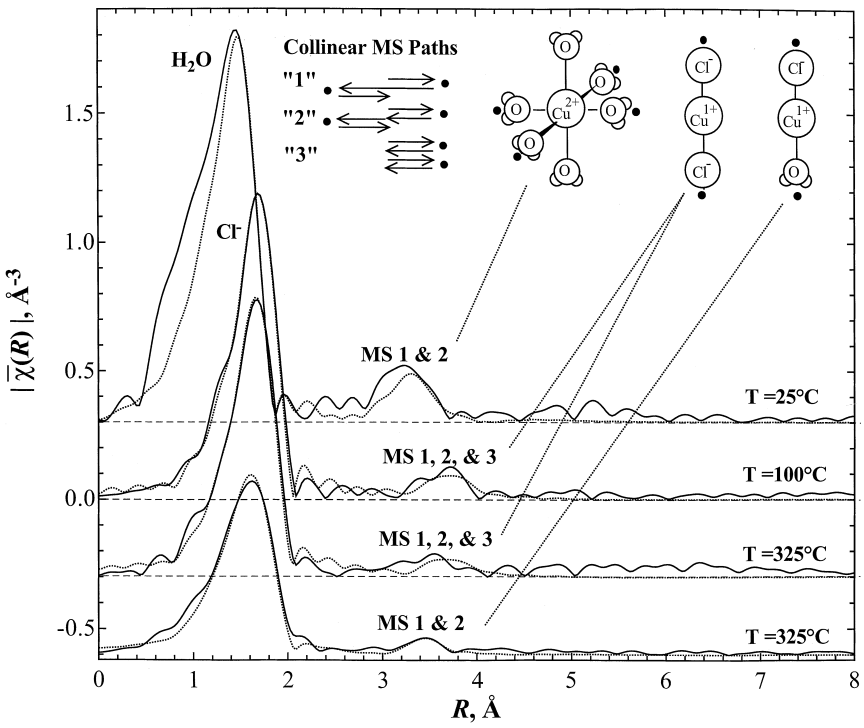

Fig. 4. The $|\tilde{\chi}(R)|$ plot from the magnitude of the Fourier transform $\chi(k)$ spectra shown in Fig. 3. This $|\tilde{\chi}(R)|$ plot is uncorrected for phase shifts whereas the actual distances are reported in Table 1. The solid line shows the experimental data and the dashed line shows the model fit to the data set using FEFF calculations.

the MS paths is very close to the theoretical value for a collinear structure (two times greater than the value for the SS path). Thus the existence of this MS peak is definitive evidence of a collinear arrangement of the Cl about the Cu. At 325°C the MS peak at 3.75 Å has weakened considerably, presumably because of an increase in the non-collinearity of the bond. However, even a slight amount of non-collinearity can greatly damp the MS path hence the structure must still remain primarily collinear. The $\tilde{\chi}(R)$ plot at the bottom of Fig. 4 is for the 0.4 m Cu^{1+} solution having no added NaCl. In this case, the main peak at 1.6 Å has broadened, is shifted to slightly shorter distance and is much reduced in amplitude. This is due to the presence of a small amount of water (or perhaps OH^-) with the Cl^- in the first shell. There is also a weak MS scattering peak at 3.45 Å that is tentatively assigned to a linear Cl^-–Cu–H_2O species. For structure $\mathbf{L}_b$, the two distinctly different MS '3' paths (Fig. 4) were not used in the fitting because their respective degeneracies are half that for the corresponding $\mathbf{L}_a$ path.

Table 1 lists all of the structural parameters for the Cu^{1+} and Cu^{2+} species that were derived from the fits of the theoretical standards to the experimental data. The reported values for the distances and Debye–Waller factors for the hexaaqua Cu^{2+} species under ambient conditions are in good agreement with previously reported values [24,25]. For the series of experiments listed as 'B, C, D, E, and F', excellent fits are obtained in all cases (see Figs. 3 and 4) for a structure with 2 Cl^- ions at an average distance of about 2.126 Å. This series of experiments covers a wide range of concentrations and temperatures over which there is virtually no change in the first-shell coordination structure. The presence of a two-coordinate Cu^{1+} species determined from the EXAFS region confirms results from the previously described analysis of the

XANES region. Within the experimental error (±0.006 Å), there is no change in the Cu–Cl distance at higher temperatures. The value of the Debye–Waller factor, which measures the width the first peak in the Cu–Cl pair distribution function, is relatively small for ionic interactions and indicates that the binding of the Cl^- to the Cu is quite strong. The very small fitted values of the third cumulant, C_3, reported in Table 1, indicate that there is almost no asymmetry in the shape of the first peak in the pair distribution function.

A further surprising finding for the six systems that contain an excess of Cl^- is that there are no tightly bond water molecules in the first-solvation shell about the $CuCl_2^-$ species. This is the same observation made for the structure about the $CuBr_2^-$ species at high temperatures that has been previously reported [13] and is also consistent with the observation of the structure about Cu(I) dihalides in polar organic solvents [10]. One possible explanation for the lack of tightly bound water molecules is that the Cu–Cl interaction may be partially covalent in nature which may delocalize the electron density away from the equatorial region and thereby reducing the capability for binding with water. The lack of any O coordination in the first shell also excludes the presence of hydrolysis species (OH^-) since the electrostatic attraction with Cu^{1+} would lead to tightly bound water at much shorter distance. At high temperatures, entropic changes strongly favor lowest coordination structures [28]. The chemical behavior of Cu^{1+} with its propensity to bind with only two ligands and to loose all bound water ligands in the first shell, should be strongly favored entropically at higher temperatures since many water molecules are liberated during this chemical transition.

The interpretation of the results for the 325°C Cu^{1+} solution without added NaCl (experiment 'G') is more complicated since the analysis of the data using a simple linear Cl^-–$Cu(H_2O)$ model gave marginally acceptable results. Although the SS peak at 1.6 Å and the MS peak at 3.45 Å are fit with such a model, the total coordination number of 1.3 (1.0 Cl^- and 0.3 H_2O) is less than expected for a two-coordinate species that was strongly indicated from analysis of the XANES region. The coordination species must satisfy both the overall 1:1 ratio of Cl/Cu while also satisfying the requirement of a two-coordinate Cu species. For this reason a variety of other structures were considered including different dimer and trimer species. High-temperature CuCl vapor phase measurements (CuCl melt equilibrium) via IR matrix isolation methods [29] indicate that a six-member-ring trimer species is predominate and that much higher temperatures are required to obtain the monomer and dimer species. However, fits of the experimental XAFS data to planar and distorted cyclic trimer species were not satisfactory, especially in fitting the MS peak at 3.45 Å. Various dimer species including a planar four-member ring with the formula H_2O–(Cu_2Cl_2)–H_2O and the linear dimer $ClCu(H_2O)CuCl$ that included Cu–Cu scattering paths were considered. However, the best fitting results were obtained using the linear dimer, $(H_2O)Cu$–Cl^-–Cu–Cl^-. With this dimer model there is a marginal improvement in the quality of the fits relative to the monomer model, however, the measured coordination numbers are now consistent with the restraints on the Cu/Cl stoichiometry and coordination number. In contrast to the systems having excess Cl^- where only the dihalo species was observed, the analysis of this experimental condition (G) is further complicated by the fact that there may be multiple equilibria, e.g., a solution containing a mixture of two-coordinate monomer with small polymeric species. More conditions and temperatures would help to resolve these questions.

Acknowledgements

This research was supported by the Director, Office of Energy Research, Office of Basic Energy Sciences, Chemical Sciences Division of the US Department of Energy, under contract DE-AC06-76RLO 1830. Work by J.G.D. and M.M.H. was supported by the US Department of Energy, Office of Environmental Management under Contract No. DE-AC06-76RLO 1830. The helpful comments of E.A. Stern for the interpretation of various aspects of the XAFS and XANES spectra is appreciated.

References

[1] D.M. Pfund, J.G. Darab, J.L. Fulton, Y. Ma, J. Phys. Chem. 98 (1994) 13102.
[2] S.L. Wallen, B.J. Palmer, J.L. Fulton, J. Chem. Phys. 108 (1998) 4039.
[3] B.J. Palmer, D.M. Pfund, J.L. Fulton, J. Phys. Chem. 100 (1996) 13393.
[4] J.L. Fulton, D.M. Pfund, S.L. Wallen, M. Newville, E.A. Stern, Y. Ma, J. Chem. Phys. 105 (1996) 2161.
[5] T.M. Seward, C.M.B. Henderson, J.M. Charnock, B.R. Dobson, Geochim. Cosmochim. Acta 60 (1996) 2273.
[6] K.V. Ragnarsdottir, E.H. Oelkers, D.M. Sherman, C.R. Collins, Chem. Geol. 151 (1998) 29.
[7] M.M. Hoffmann, J.G. Darab, B.J. Palmer, J.L. Fulton, J. Phys. Chem. A 103 (1999) 8471.
[8] T.M. Seward, C.M.B. Henderson, J.M. Charnock, T. Driesner, Geochim. Cosmochim. Acta 63 (1999) 2409.
[9] R.A. Mayanovic, A.J. Anderson, W.A. Bassett, I.-M. Chou, J. Synchrotron Radiat. 6 (1999) 195.
[10] I. Persson, M. Sandström, A.T. Steel, M.J. Zapatero, R. Åkesson, Inorg. Chem. 30 (1991) 4075.
[11] B.W. Mountain, T.M. Seward, Geochim. Cosmochim. Acta 63 (1999) 11.
[12] Z. Xiao, C.H. Gammons, A.E. Williams-Jones, Geochim. Cosmochim. Acta 62 (1998) 2949.
[13] J.L. Fulton, M.M. Hoffmann, J.G. Darab, B.J. Palmer, E.A. Stern, J. Phys. Chem. A, 2000 (in press).
[14] M.M. Hoffmann, J.G. Darab, S.M. Heald, C.R. Yonker, J.L. Fulton, Chem. Geol. 167 (2000) 89.
[15] J.L. Fulton, J.G. Darab, M.M. Hoffmann, Rev. Sci. Instrum., 2000 (submitted).
[16] B.K. Teo, EXAFS: Basic Principles and Data Analysis, Springer, New York, 1986.
[17] E.A. Stern, S. Heald, Handbook of Synchrotron Radiation, in: D.E. Eastman, Y. Farge, E.E. Koch (Eds.), North-Holland, Amsterdam, 1983.
[18] D.C. Koningsberger, R. Prins (Eds.), X-Ray Absorption: Principles, Applications, Techniques of EXAFS, SEXAFS and XANES, Wiley, New York, 1988.
[19] E.A. Stern, M. Newville, B. Ravel, Y. Yacoby, D. Haskel, Physica B 208/209 (1995) 117.
[20] S.I. Zabinsky, J.J. Rehr, A. Ankudinov, R.C. Albers, M.J. Eller, Phys. Rev. B. 52 (1995) 2995.
[21] M. Newville, R. Ravel, D. Haskel, J.J. Rehr, E.A. Stern, Y. Yacoby, Physica B 208/209 (1995) 154.
[22] L.-S. Kau, D.J. Spira-Solomon, J.E. Penner-Hahn, K.O. Hodgson, E.I. Solomon, J. Am. Chem. Soc. 109 (1987) 6433.
[23] I.J. Pickering, G.N. George, Inorg. Chem. 34 (1995) 3142.
[24] P. D'Angelo, E. Bottari, M.R. Festa, H.-F. Nolting, N.V. Pavel, J. Chem. Phys 107 (1997) 2807.
[25] G.V. Korshin, A.I. Frenkel, E.A. Stern, Environ. Sci. Technol. 32 (1998) 2699.
[26] S. Ansell, R.H. Tromp, G.W. Neilson, J. Phys. 7 (1995) 1513.
[27] M.D. Collings, D.M. Sherman, K.V. Ragnarsdottir, Chem. Geol. 167 (2000) 65.
[28] R.E. Mesmer, W.L. Marshall, D.A. Palmer, J.M. Simonson, H.F. Holmes, J. Solution Chem. 17 (1988) 699.
[29] T.P. Martin, H. Schaber, J. Chem. Phys. 73 (1980) 3541.